Start-up shear of spherocylinder packings: Effect of friction

Claus Heussinger

Institute for Theoretical Physics, Georg August University Göttingen, Friedrich Hund Platz 1, 37077 Göttingen, Germany

We study the response to shear deformations of packings of long spherocylindrical particles that interact via frictional forces with friction coefficient μ. The packings are produced and deformed with the help of molecular dynamics simulations combined with minimization techniques performed on a GPU. We calculate the linear shear modulus g_∞, which is orders of magnitude larger than the modulus g_0 in the corresponding frictionless system. The motion of the particles responsible for these large frictional forces is governed by and increases with the length ℓ of the spherocylinders. One consequence of this motion is that the shear modulus g_∞ approaches a finite value in the limit $\ell \to \infty$, even though the density of the packings vanishes, $\rho \propto \ell^{-2}$. By way of contrast, the frictionless modulus decreases to zero, $g_0 \sim \ell^{-2}$, in accordance with the behavior of density. Increasing the strain beyond a value $\gamma_c \sim \mu$, the packing strain weakens from the large frictional to the smaller frictionless modulus when contacts saturate at the Coulomb inequality and start to slide. In this regime, sliding friction contributes a "yield stress" $\sigma_y = g_\infty \gamma_c$ and the stress behaves as $\sigma = \sigma_y + g_0 \gamma$. The interplay between static and sliding friction gives rise to hysteresis in oscillatory shear simulations.

I. INTRODUCTION

In this work we deal with the linear elastic properties of packings of long rodlike particles. Assemblies of this sort occur in a variety of different systems from wool fibers in felt and other textiles, rods in filter applications, or as reinforcement, to micro- and nanosized systems, like fd-virus colonies or semiflexible biopolymers in tissue and the cytoskeleton. Aspect ratios and interaction forces are manifold. In macroscopic systems, frictional forces are essential (e.g., to hold textiles together). In cytoskeletal systems one has Brownian forces and protein-mediated adhesion (bonding) between the fibers.

Here, we are interested in the effects of frictional forces on the elastic shear modulus of a packing of non-Brownian spherocylindrical particles (see Fig. 1). A spherocylinder (SC) consists of a cylinder and two hemispherical caps at the two ends. In a previous publication [1] we have dealt with the same system, but in the absence of friction. Steric hindrance plays a crucial role for the motion of particles, which are tightly caged by their neighbors. Motion along the long cylinder axis, however, is not restrained by the surrounding. This motion induces sliding of the contacts on the surface of the cylinders and is expected to give rise to large frictional forces. We therefore expect friction to modify the shear modulus dramatically.

Packings of nonspherical particles have received considerable attention in recent years. In particular, the question of maximally dense packings has been the subject of works on particles of various shapes [2]. Most of these particles are rather compact and more or less spherelike, quite different from the long, thin rods discussed in this contribution. Increasing the length of the rods from zero, packing densities reach a maximum [3,4] before dropping steadily. Assembled

in random fashion, long rods make rather dilute packings, with the density decreasing with particle length as $\rho \propto \ell^{-2}$ [5]. In terms of particle volume fraction $\phi = \rho V_{sc}$ the dependence is $\phi \propto \ell^{-1}$. This is a consequence of the different scaling of particle volume V_{sc} and excluded volume [6] with diameter d and length ℓ of rodlike particles

$$V_{sc} \sim d^2 \ell, \quad V_{excl} \sim d\ell^2. \tag{1}$$

Neglecting correlations between particles (random contact model, Ref. [5]) the average number of contacts of a particle is

$$z \sim N \frac{V_{excl}}{V} = \phi \frac{V_{excl}}{V_{sc}}. \tag{2}$$

With the number of contacts fixed at the jamming threshold z_c one gets for the jamming density

$$\phi \sim \frac{z_c d}{\ell}. \tag{3}$$

Measured values for z_c range from approximately 8 to 10 [4,5,7,8]. The latter value represents the classical Maxwell counting [9] for particles with one rotational symmetry. The reduced value of 8 results when translations along the long axis are also regarded as a symmetry [1]. In that paper it was shown that these two limiting cases can be combined by a more general counting procedure that accounts for the fraction f of spherocylinders with end contacts (both ends need to be constrained). This can be written in analogy to Eq. (2) as

$$f \sim \left(N \frac{V_{sc}}{V} \right)^2 \sim \phi^2. \tag{4}$$

End contacts break the translational symmetry such that the jamming threshold in terms of the contacts is $z_c = 8 + 2f$.
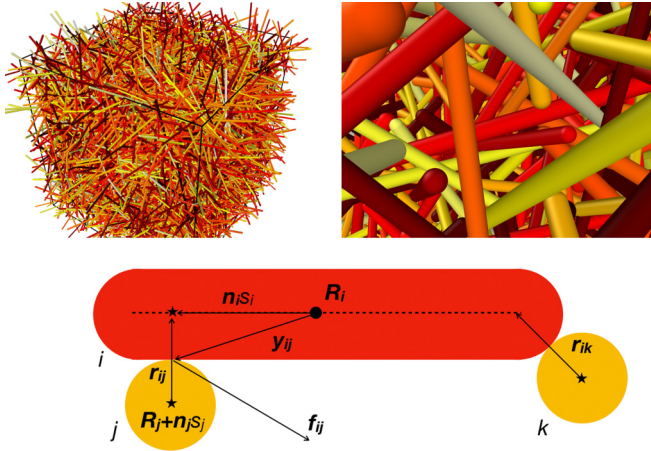
FIG. 1. Top: packing of 6144 spherocylinders with aspect ratio $\alpha = 40$. Volume fraction $\phi = 0.1$, i.e., 90% of space is empty. Zoom into packing illustrates these large voids. Color signals orientation. Pictures prepared with OVITO. Bottom: sketch illustrating the interaction between spherocylinders. Particle i is projected into the drawing plane, while particles j and k are oriented perpendicular to this plane. Therefore, they appear as circles. Particle j is a side contact to i, particle k an end contact.

Previous work on packings of fibers and rods is mainly computational. Statistical properties of packings of rods are calculated in [3,4,10]. Meng *et al.* [11] highlight the dependence on the amount of order in the packing, while [12] shows that order may develop in response to repeated tapping. Bending flexibility is introduced either within bead-spring models [7,13] or by coupling rigid rods together [14,15].

Experimental approaches to measure density in rod packings are presented in [5,16]; Ref. [8] even manages to determine the number of contacts. Ekman *et al.* [17] highlight a correlation effect that goes beyond the random contact model of Ref. [5] and that shows up in the distribution of contacts.

Going beyond static packings rheological properties are discussed in a variety of contexts. Some computational approaches are reviewed in [18]. Steady shear in systems of short spherocylinders has been studied in Nath *et al.* [19]. A key finding was that frictional interaction forces suppress alignment during shear. Similar systems have been studied in three [20,21] and two spatial dimensions [22–24]. Experimental work frequently considers the interplay of (frictional) contact and hydrodynamic forces in suspensions [25–28].

Here, we are concerned with the response of rod packings to small deformations, within the linear regime. Particular emphasis is put on the relevance of frictional forces. A related study was presented in Ref. [15] that deals with compressed packings of elastic fibers that can bend and stretch. It turns out that packings without friction have a negligible shear modulus as compared to frictional packings. In the following, we will present a similar phenomenon in packings of rigid rods. By carefully evaluating the dependence on rod length, we find the origin of the large frictional modulus, and explain it in terms of the dominant deformation modes.

II. MODEL

We study three-dimensional (3D) packings of spherocylindrical particles $i = 1 \ldots N$ of length ℓ_i and diameter d_i. All particles of the packing have the same aspect ratio $\alpha = \ell_i/d_i$. The particles interact via repulsive contact forces similar to those from models for spheres. A contact between particles i and j is established whenever the shortest distance between the backbones, $r_{ij} = |\mathbf{r}_{ij}|$, is less than their average diameter $d_{ij} = (d_i + d_j)/2$.

The distance vector can be written as

$$r_{ij}\hat{\mathbf{e}}_{ij} = \mathbf{R}_i + \hat{\mathbf{n}}_i s_i - (\mathbf{R}_j + \hat{\mathbf{n}}_j s_j), \quad (5)$$

where $\mathbf{R}_i$ is the position of the center of mass of particle i, $\hat{\mathbf{n}}_i$ represents the direction of the particle backbone, and $s_i \in [-\ell_i/2, \ell_i/2]$ is the arclength parameter along the backbone that specifies where the shortest distance between i and j is reached. By definition the direction of the contact $\hat{\mathbf{e}}_{ij}$ is perpendicular to both backbones ($\hat{\mathbf{e}}_{ij} \cdot \hat{\mathbf{n}}_{i/j} = 0$), except for cases where the shortest distance is reached at an end of one or both of the SC (i.e., $s_i = \pm\ell_i/2$). The actual force is applied halfway along the vector $\mathbf{r}_{ij}$ at $\mathbf{y}_{ij} = \hat{\mathbf{n}}_i s_i + \mathbf{r}_{ij}/2$ away from the center of mass (with a small correction for unequal-sized particles). This is, in general, very close to the surface of the two particles.

The force $\mathbf{f}_{ij}$ on particle i from the contact with j has components normal $\mathbf{f}_{ij}^n$ and tangential $\mathbf{f}_{ij}^t$ to the particle surface. They are calculated as in the Cundall-Strack model [29]

$$\mathbf{f}_{ij}^n = \left[-k_n \delta_{ij} \hat{\mathbf{e}}_{ij} - c_n \mathbf{v}_{ij}^n \right],$$
$$\mathbf{f}_{ij}^t = \left[-k_t \boldsymbol{\xi}_{ij}^t - c_t \mathbf{v}_{ij}^t \right]. \quad (6)$$

Here, the normal direction $\hat{\mathbf{e}}_{ij} = \mathbf{r}_{ij}/r_{ij}$ points from particle j to i at the point of application of the force. The normal overlap $\delta_{ij} = d_{ij} - r_{ij}$ is a positive quantity. The tangential overlap $\boldsymbol{\xi}_{ij}^t$ is the displacement tangential to the surface of the SC, which accumulates during the lifetime of the contact. The relative velocity $\mathbf{v}_{ij}^{\text{con}}$ at the contact is split into normal $\mathbf{v}_{ij}^n$ and tangential components $\mathbf{v}_{ij}^t$. It derives from the center-of-mass translational $\mathbf{v}_i$ and rotational motion $\boldsymbol{\omega}_i$ as $\mathbf{v}_{ij}^{\text{con}} = (\mathbf{v}_i - \mathbf{v}_j) - \mathbf{y}_{ij} \times \boldsymbol{\omega}_i + \mathbf{y}_{ji} \times \boldsymbol{\omega}_j$.

The parameters k_n and k_t are spring constants; c_n and c_t are viscous damping constants. Solid sliding friction is taken into account replacing $\mathbf{f}^t$ by $\mu|\mathbf{f}^n|(\mathbf{f}^t/|\mathbf{f}^t|)$, whenever the Coulomb inequality

$$|\mathbf{f}^t| < \mu|\mathbf{f}^n| \quad (7)$$

is violated. We also consider the frictionless limit $\mu = 0$, in which case we still keep the tangential viscous force $\propto c_t$.

The equations of motion for particle i are

$$m\ddot{\mathbf{R}}_i = \sum_j \mathbf{f}_{ij}, \quad (8)$$

$$\mathbf{I}_i \cdot \dot{\boldsymbol{\omega}}_i = \sum_j \mathbf{y}_{ij} \times \mathbf{f}_{ij}, \quad (9)$$

where $\mathbf{I}_i$ is the moment of inertia of particle i calculated for a spherocylinder with a homogeneous mass density.

We have set $k_n = 1$, $k_t/k_n = 2/7$, $c_n = 0.5$, and $c_t/c_n = 0.1$. These values are standard choices. In particular, c_n is

chosen such that damping is sufficiently strong without leading to overdamped motion. For truly elastic response, the values of the dissipative coefficients do not matter. All particles have the same mass $m = 1$ and aspect ratio $\alpha = \ell/d$. Half of the particles have $d = 1$ and the other half have $d = 1.4$. System sizes are chosen such that the linear dimension of the simulation box is at least three times the length of the simulated SC. The unit of energy density (stress or modulus) is k_n/d. Times are expressed in units of the elastic collision time $\sqrt{m/k_n}$.

III. RESULTS: RESPONSE TO SHEAR

A. Preparing packings for shear deformation

A stable, i.e., force-equilibrated, packing of SCs of a given aspect ratio (see Fig. 1) is produced with the help of the FIRE minimization [30]. During this initial minimization no dissipative nor frictional forces are present, i.e., $k_t = c_t = c_n = 0$. The response of such frictionless packings to quasistatic shear has been studied in Ref. [1]. Here we are interested in how frictional forces modify the response. Thus, after minimization, frictional forces with parameters specified above are turned on, while the simulation box is deformed at a constant strain rate $\dot{\gamma} = 10^{-7}$. Lees-Edwards boundary conditions [31] are used here. The strain rate needs to be chosen small enough to reproduce the quasistatic results at zero friction, $\mu = 0$. We have checked that this is the case; see, e.g., Fig. 6. For the linear response properties only small strains $\Delta\gamma \approx 10^{-4}$ are needed.

B. Large friction limit: $\mu \to \infty$

If μ is infinite, the Coulomb inequality, Eq. (7), is ineffective and provides no restriction on the frictional forces $\mathbf{f}^t$. A frictional interaction force at a contact then acts similar to a conservative force from an elastic bond with spring constant k_t (neglecting a small effect from c_t). The magnitude of the tangential displacement $\boldsymbol{\xi}^t$ then represents the extension of this spring. This limit is achieved when the response does not change anymore with μ. Here we use $\mu = 10$.

The stress is calculated from the virial expression [23,32]

$$\sigma = \frac{1}{V}\sum_{k<l} f_{kl}^x R_{kl}^y = \frac{Nz}{2V}\langle f^x R^y \rangle_c, \tag{10}$$

where the latter expression denotes an average over all contacts N_c with $z = 2N_c/N$ the average number of contacts per SC. Due to the relation $\mathbf{R_{kl}} = \mathbf{R_k} - \mathbf{R_l} = \mathbf{y_{kl}} - \mathbf{y_{lk}}$ one may also write the stress in terms of the lever arms as $\sigma = \frac{1}{V}\sum_{k,l} f_{kl}^x y_{kl}^y$. From the stress-strain relation $\sigma(\gamma)$ at small strains the linear shear modulus is calculated as the slope, $g = d\sigma/d\gamma$. In Fig. 2, $g_\infty = g(\mu \to \infty)$ is plotted for various configurations with different spherocylinder aspect ratio $\alpha = \ell/d$ and volume fraction ϕ. As the control parameter the contact number z is used.

The moduli can be fit to the form $g \sim z - z_0$ with z_0 ranging between 6 and 6.5 depending on the aspect ratio. However, it is also possible to fit all different α with one $z_0 \approx 6.5$. This threshold value is larger than the frictional jamming limit $z_J = 4$. As our packings are produced by energy minimization in 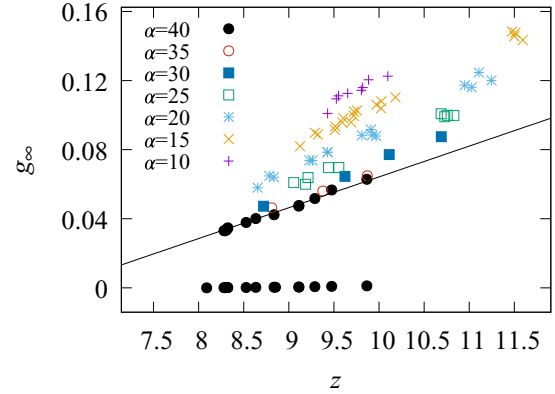the absence of friction, they necessarily have a contact number $z > 8$. As soon as the coordination drops markedly below this value, energy minimization takes the packing to $z \to 0$. Thus the threshold z_0 cannot be reached by using our protocol. It might be interesting to study different packing-generation protocols in order to reach to lower z.

FIG. 2. Shear modulus g_∞ vs contacts z for infinite friction $\mu \to \infty$ and various aspect ratios. Line is a fit $g \sim (z - z_0)$ to the data with $\alpha = 40$. The data points at nearly zero correspond to the frictionless limit ($\alpha = 40$), where the modulus is on the order of 10^{-4}.

Comparing with the frictionless limit $\mu = 0$ (see data points at nearly zero, or Fig. 6 in Ref. [1]), the infinite-friction modulus is two to three orders of magnitude larger. Similarly large differences between frictional and frictionless moduli have been observed in simulations of nonbonded fibrous materials [15].

Also the α dependence is different. The zero-friction modulus g_0 vanishes in the long-SC limit, as $g_0 \sim \alpha^{-2}$ [1]. On the other hand, g_∞ shows hardly any dependence on α (Fig. 2), at least in the large α limit.

SC length $\ell = \alpha d$ may enter the stress, Eq. (10), and thus the modulus in various ways. The first contribution comes from stress being an energy *density*. The normalization with density N/V can be written as $N/V = \phi/V_{sc}$ and, using Eqs. (1) and (3), as $(d/\ell)/(d^2\ell) \sim \ell^{-2}$. This alone would explain the result $g_0 \sim \ell^{-2}$ of the frictionless system.

However, additional ℓ dependence may come from the force-position correlator part of the stress $\langle f_x R_y \rangle$. One contribution is the force, or the magnitude of the overlaps δ and $\boldsymbol{\xi}^t$, and their change with strain; see Eq. (6). The normal overlaps δ are the only contribution in the frictionless system, and give rise to g_0. In the frictional system also the tangential overlaps $\boldsymbol{\xi}^t$ are present. They measure how much the positions of contacts move on the surface of the SCs, in other words, how strongly SCs are sliding relative to each other. Such sliding motion gives rise to frictional forces and thus to g_∞.

In Figs. 3(a) and 3(b) we display the mean-square tangential overlap $\delta_t^2 \equiv \langle \boldsymbol{\xi}^t \cdot \boldsymbol{\xi}^t \rangle$. We find $\delta_t \propto \gamma$, such that frictional contacts move at constant velocity $v_t = \delta_t/t \propto \dot{\gamma}$. This velocity, at least for large α, is $\propto \ell$ as Fig. 3(b) shows. Thus $\delta_t \propto \ell\gamma$ ($v_t \propto \ell\dot{\gamma}$) and tangential displacements of contacts per unit of strain grow with the length ℓ of the SC. The displacements are, in particular, independent of the SC diameter d, which is the alternative length scale that might show up. On the other
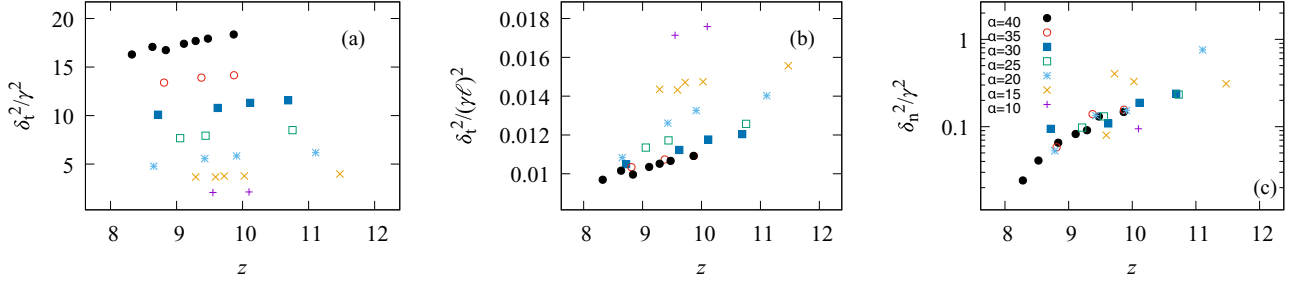
FIG. 3. (a) Mean-square tangential overlap $(\delta_t/\gamma)^2$ vs contacts z for infinite friction $\mu \to \infty$ and various aspect ratios. (b) Same data, now rescaled by $\gamma\ell$; (c) mean-square normal overlap $(\delta_n/\gamma)^2$.

hand, the normal overlaps $\delta_n^2 = \langle\delta^2\rangle$ are independent of SC length, as panel 3(c) shows. They thus scale as $\delta_n \propto d\gamma$.

Finally, there is also an ℓ dependence in the position part of the correlator, which is the center-of-mass distance between the two overlapping SCs [see Eq. (5)]

$$\mathbf{R}_{ij} = r_{ij}\hat{\mathbf{e}}_{ij} - \hat{\mathbf{n}}_i s_i + \hat{\mathbf{n}}_j s_j, \tag{11}$$

where the ℓ dependency is carried by the arc-length parameters s_i and s_j.

In the case of pressure ($p \sim \langle\mathbf{f} \cdot \mathbf{R}\rangle$) it is easy to see that this latter part does not contribute in the frictionless scenario. There the force is normal to the surface, $\mathbf{f} \parallel \hat{\mathbf{e}}$, and thus perpendicular to the long axis given by $\hat{\mathbf{n}}$. The s_i, s_j terms therefore drop out. The same result is expected for the shear stress, as long as one assumes statistical independence between the orientation of the SC, $\hat{\mathbf{n}}$, and the orientation of the contact with its neighbors. In the frictional scenario, on the other hand, the force is tangential to the surface; thus the s terms survive.

Taking all these dependencies together one expects $g_0 \sim z(\phi/d^2\ell)k_n d^2 \sim (k_n/d)(d/\ell)^2$ (Ref. [1]) and $g_\infty \sim z(\phi/d^2\ell)k_t\ell^2 \sim (k_t/d)$ (Fig. 2).

Looking at Fig. 2 one may also get the impression that the modulus slowly decreases with SC length. In fact, one can approximately collapse the data assuming $g_\infty \sim \alpha^{-1/2}$. However, this apparent scaling is an artifact of the limited range of available α. To justify this claim, we consider only the side

contacts in the calculations of the modulus. This modulus g_s is displayed in Fig. 4. In the limit $\alpha \to \infty$ the side contacts make the only contribution to the modulus as no end contacts occur. One clearly sees that this contribution is independent of α, at least for the longest spherocylinders. Thus we can safely assume that this value g_s, which is only slightly smaller than the full modulus g_∞ (thin line, taken from Fig. 2), represents the finite full modulus in the $\alpha \to \infty$ limit. In consequence, the scaling with $\alpha^{-0.5}$ cannot be true.

Finally, in Fig. 5 we also consider the motion of particles (as compared to the motion of contacts as given by δ_t). In response to the imposed strain γ, particles on average move in shear direction (x) by an amount γY, depending on the coordinate of the particle in the gradient direction (y). In gradient or vorticity direction there is no average motion. But fluctuations are present. In the figure we display the magnitude of fluctuating motion in gradient direction, $\delta_y(\gamma)^2 = \sum_i [Y_i(\gamma) - Y_i(0)]^2/N$. At the small strains studied we find $\delta_y(\gamma)^2 \propto \gamma^2$. A different, e.g., diffusive, behavior may only be expected at much larger strains. Fluctuations in vorticity direction are of roughly the same magnitude. As the figure shows, the fluctuations of the motion of particles, similar to the displacements of contacts, scales with ℓ. Noteworthy is that also the magnitude of both is quite similar, $\delta_y \approx 0.05\gamma\ell$, to be compared with contact displacements $\delta_t \approx 0.1\gamma\ell$.

C. Finite friction coefficient $\mu < \infty$

The infinite friction coefficient is rather unrealistic for any real material. Here, we report results for varying friction
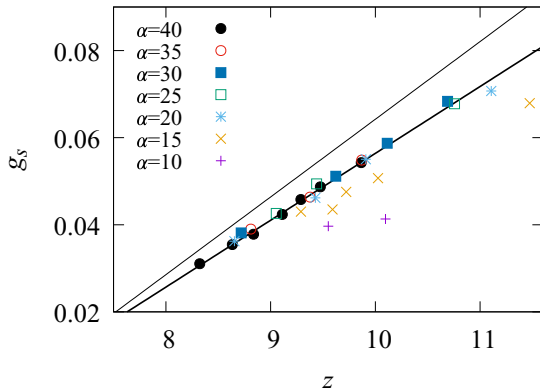

FIG. 4. Shear modulus of the side contacts g_s vs z for infinite friction $\mu \to \infty$ and various aspect ratios. Thin solid line full shear modulus (from Fig. 2) for the longest SC with $\alpha = 40$. Thick solid line fit to the data with $\alpha = 40$.
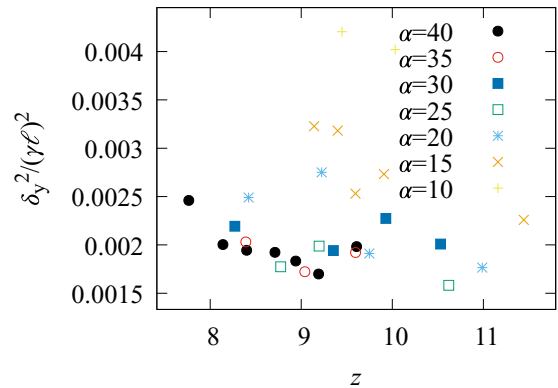

FIG. 5. Fluctuations of SC center-of-mass displacement in gradient direction $(\delta_y/\gamma)^2$ vs z.
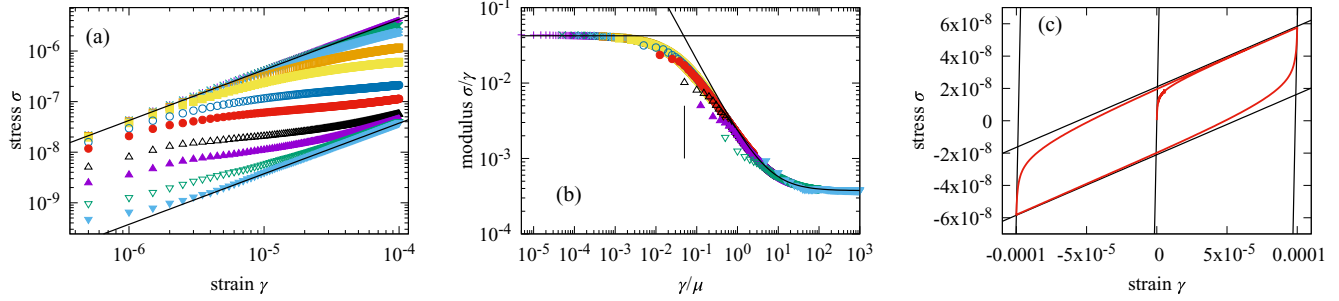
FIG. 6. (a) Stress vs strain for various $\mu = 1 \ldots 10^{-7}$ (from top to bottom) and $\alpha = 40$, $\phi = 0.11$. Lines represent limits of infinite (top) and zero (bottom) friction coefficient, respectively. (b) Modulus σ/γ vs rescaled strain γ/μ for the same data. Solid lines: infinite-friction modulus and yield-stress model for zero friction $\sigma = g_0\gamma + g_\infty\gamma_c$. Vertical line: crossover value $\gamma/\mu = 0.05$ as derived in the text. (c) Strain cycle with maximum strain $\gamma_0 = 10^{-4}$ and $\mu = 10^{-5}$. Lines represent limits of infinite and zero friction coefficient, shifted appropriately.

coefficients, spanning the range from nearly frictionless ($\mu \approx 0$) to the infinite-friction scenario of the first section. Figure 6 presents the stress-strain relation for different μ of one particular packing with $\alpha = 40$. For small strain the stress follows the infinite-μ line $\sigma = g_\infty\gamma$, then saturates in a quasiplateau before approaching the frictionless response $\sigma = g_0\gamma$. The strain γ_c where this change in behavior occurs depends on μ.

At strains $\gamma < \gamma_c$, the external work $V\sigma\dot{\gamma}$ is converted into "potential" energy of the tangential spring k_t: $dE_{\text{pot}}/dt \sim Nzk_t\ell^2\gamma\dot{\gamma}$. The stress here is $\sigma = g_\infty\gamma$ with the infinite-friction modulus $g_\infty \sim (\phi z/\ell)k_t\ell^2$, with the prefactor assuring an ℓ-independent modulus, as discussed above.

The crossover scale to the quasiplateau can be expected to depend on the saturation of the Coulomb inequality, Eq. (7), as equality, $f_t = \mu f_n$. At this point contacts start to slide, which enters work-energy balance as an additional dissipative term, $\Gamma_t \sim Nz\mu f_n v_t$.

With the normal force set by pressure, $f_n \sim p\ell/z\phi$, we find for the crossover strain

$$\gamma_c \sim \frac{\mu p}{k_t z\phi}. \tag{12}$$

Indeed, all data collapse to a unique scaling form when plotted vs a rescaled strain γ/μ [Fig. 6(b)]. Respecting all the numerical factors for this set of data, Eq. (12) gives a crossover strain $\gamma_c = 0.05\mu$ [indicated by the vertical line in panel 6(b)].

For strains $\gamma > \gamma_c$ the relevant potential energy is that of the normal overlaps, $dE_{\text{pot}}/dt \sim Nzk_n\gamma\dot{\gamma}$, and the stress becomes $\sigma \sim \sigma_y + g_0\gamma$ with the zero-friction modulus $g_0 \sim (\phi z/\ell)k_n d^2$ and the "yield stress" $\sigma_y \sim g_\infty\gamma_c \sim \mu p\ell$. Thus, at large strains, the frictional forces contribute a yield stress $\sigma_y \sim g_\infty\gamma_c \sim g_\infty\mu$ to the frictionless response.

At zero strain the modulus is expected to reach the μ-independent value g_∞. Deviations from this expectation and a lack of scaling are visible in Fig. 6(b) for some data sets, which seem to level off at lower values. This, however, is an artifact from a too large deformation rate $\dot{\gamma} = 10^{-7}$. We have checked that by reducing the strain rate to 10^{-8} no deviations from scaling occur within the range of strains studied.

To wrap up, long spherocylinders respond to strain primarily via sliding. Contacts are displaced in surface-tangential direction by amounts $\delta_t \sim \gamma\ell$. As a consequence, frictional forces $f_t = k_t\delta_t$ increase and dominate the elastic modulus. Nonfrictional forces f_n, directed normal to the SC surface,

increase much slower and constitute only a small part of the total modulus. At strains $\gamma_c \propto \mu$ the Coulomb threshold of the contacts is reached and frictional forces cannot increase further. The stress first reaches a plateau before, eventually, the normal forces start to dominate the response. From this point the packing behaves as if it were frictionless with a yield stress (the plateau) from the frictional forces $\sigma_y \sim g_\infty\mu$. Still, energy is dissipated because contacts are sliding. This gives rise to hysteresis in oscillatory sweeps. To probe this we perform oscillatory strains $\gamma(t) = \gamma_0\sin(\omega t)$ [Fig. 6(c)] with variable maximal strain γ_0 and frequency ω chosen such that the product $\gamma_0\omega$ matches the strain rates used up to now. Friction governs the response (highlighted by the steep lines $\sigma = g_\infty\gamma$) in the startup, as well as just after strain reversal. After reversal the frictional sliding stops and contacts stick. The tangential springs relax and load in the opposite direction. Once the sliding limit in this direction is reached, a crossover to frictionless response (shallow lines $\sigma = g_0\gamma$) is observed again.

D. Viscous dissipation

Dissipation is due to sliding friction of the contacts. Technically, this is due to the application of the Coulomb inequality, Eq. (7), which effectively rescales ξ^t to keep tangential forces from increasing beyond what is allowed by the inequality. This leads to a loss of energy. This mechanism is strain rate independent and is therefore called "plastic dissipation." The rescaling also implies that c_t, i.e., the viscous dissipation in the tangential motion, is not relevant; it is the total tangential force, including the viscous component, that is limited according to Coulomb inequality. To assess the influence of viscous dissipation on the response we therefore study the frictionless limit $\mu = 0$ in combination with different values of c_t, which governs the strength of viscous dissipation due to relative sliding motions. The tangential force, Eq. (6), reduces to $\mathbf{f}_t = -c_t\mathbf{v}_t$.

Figure 7 compares the stress-strain relations for one particular packing sheared at various strain rates and with different values of c_t. For comparison the quasistatic result, for which the parameter c_t is irrelevant, is also displayed.

The data indicate the scaling form $\sigma = c_t\dot{\gamma}F(t/c_t)$, with $F(x \to \infty) \to x$ or $F(x \to 0) \to x^\epsilon$ and small exponent $\epsilon \approx 0.13$. An $\epsilon = 0$ would give $\sigma = c_t\dot{\gamma}$ in the initial regime,
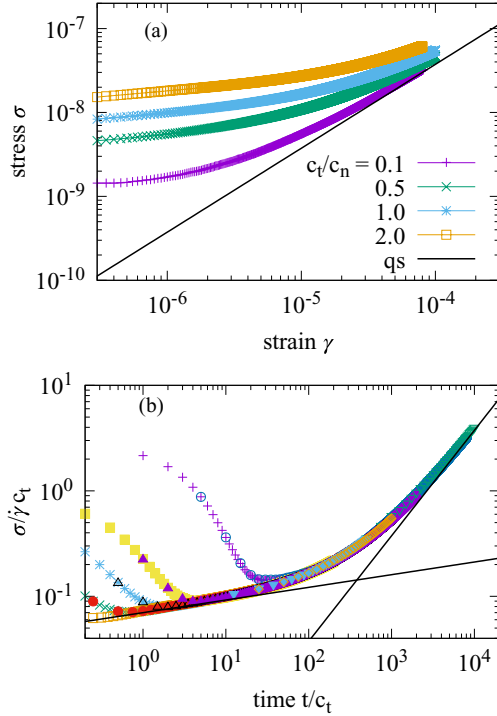
FIG. 7. (a) Stress vs strain for various $c_t/c_n = 0.1 \ldots 4.0$, $c_n = 0.5$ and $\alpha = 40$, $\phi = 0.11$, $\mu = 0$, $\dot{\gamma} = 10^{-7}$. Line represents quasistatic results; see Fig. 6. (b) Rescaled stress $\sigma/(\dot{\gamma} c_t)$ vs time t/c_t for the same data, as well as different strain rates, $\dot{\gamma} = 10^{-6}, 10^{-8}$. Dotted line $\sim x^\epsilon$, $\sim x$.

which indicates dissipation via tangential viscous forces when contacts are sliding with velocities set by the strain rate $v_t \sim \ell \dot{\gamma}$. In more detail, the energy-work balance has three terms

$$Nzk_n\gamma\dot{\gamma} = V\sigma\dot{\gamma} - Nzc_t\langle v_t^2 \rangle. \tag{13}$$

The terms are the time rate of change of the potential energy, the external work, and the dissipation now via viscous forces. At early times one balances stress with dissipation to obtain $\sigma \sim (\phi z/\ell)c_t\dot{\gamma}\ell^2$, i.e., a time-independent constant. This is the regime, where, in our data, we still see a weak time dependence, governed by the exponent ϵ. For the velocities this would imply a time dependence $v_t \sim (t/c_t)^{\epsilon/2}\ell\dot{\gamma}$. At long times the usual elastic regime $\sigma = g_0\gamma$ sets in. The crossover time scale is $\tau \sim z^2 c_t/g_0$. At very short times $t \sim 1$, the scaling with $(t/c_t)^\epsilon$ breaks down. This corresponds to the elastic collision time scale, i.e., the very first collision when initial conditions are still important. In the figure this is visible as the hump at small times.

IV. DISCUSSION

We have dealt with assemblies of long spherocylinders (SC). Because of the large excluded volume of such high-aspect ratio particles, packings are of very low volume fraction that decreases with particle length as $\phi \propto \ell^{-1}$.

The key question we posed was in how far frictional forces modify or dominate the elastic response at small strains. The starting point was the assumption that steric hindrance is the

key factor to restrict particle motion. Free motion is then only possible along the long axis of the cylinder. This motion induces sliding of the contacts on the surface of the cylinders and gives rise to large frictional forces.

We have argued that frictional contact forces act similar to forces from an elastic bond, at least as long as the Coulomb threshold is not yet reached. In this analogy the motion of a contact on the surface is comparable to the extension of a permanent elastic bond (here described via a spring constant k_t). Such permanent bonds frequently occur in biological systems, e.g., the cytoskeleton, where the long filamentous or rodlike polymers are chemically or electrostatically bonded via crosslinking proteins [33,34]. Depending on the stiffness of the bonding and the polymers' intrinsic elasticity the described mechanism of contact sliding and bond extension might also lead to secondary (stretching, bending) deformations in the polymers [35–37]. Note that the spherocylindrical particles used here do not have these degrees of freedom; they are modeled as cylinders with a straight backbone that may not change length. Biopolymers in cytoskeletal systems usually have very high aspect ratios with diameters in the nanometer range and lengths exceeding the μm scale. For rodlike microtubules, however, with a diameter of $d \approx 25$ nm and lengths $\ell \approx \mu$m our simulations with $\alpha = 40$ are within physically reasonable values also for these particles.

We have determined the shear-induced tangential motion δ_t of contacts on the surface of particles (the extension of the "bonds") in a variety of packings with spherocylinders of different lengths ℓ. Interestingly, $\delta_t \propto \ell$ and thus increases with the length of the particles. This can be understood by assuming the packing to respond affinely to an imposed shear deformation γ. From the properties of an affine map, the distance between the center of mass of two SCs should change in proportion to their distance. Overlapping SCs have distances on the order of their length ℓ, such that also the change in distance is $\Delta\ell \propto \gamma\ell$. As the SCs themselves do not change length, the motion of the center of mass gives rise to relative sliding motion of the contacts of exactly this order of magnitude, $\delta_t \propto \gamma\ell$. While we have seen (Fig. 5) that the actual motion of the SCs also includes a substantial fluctuating component, this additional component also scales with ℓ. Thus the overall scaling $\delta_t \propto \ell$ is not affected, albeit the prefactor is changed.

The shear modulus itself has a finite (nonzero) limit for large ℓ. We have shown that this results from the combined effect of increasing δ_t and decreasing overall density ϕ. On the other hand, the modulus in the absence of friction is orders of magnitudes smaller and vanishes as $g_0 \propto \ell^{-2}$. Contact motion responsible for forces in this frictionless limit is normal to the surface of the particles, δ_n. Without friction, tangential motion δ_t does not build up forces. We find that δ_n is much smaller than δ_t and does not scale with the length of the SCs but their diameter, $\delta_n \sim d$.

As the strain increases frictional forces reach the limit set by the Coulomb inequality Eq. (7). At this point the packing starts to strain weaken and the shear modulus decreases to its frictionless value g_0. This generally happens at strains $\gamma_c \sim \mu p/k_t z\phi \sim \mu/\ell$, with the latter representing the limiting behavior for long SCs. At these strains, hysteresis is

observed in oscillatory sweeps $\gamma(t) = \gamma_0 \sin(\omega t)$. This highlights the presence of energy dissipation in the sliding contacts and evidences a transition from static ($\gamma < \gamma_c$) to dynamic friction ($\gamma > \gamma_c$).

Finally, we also consider energy dissipation via viscous forces, embodied in the parameter c_t. With the assumption of time-independent velocities $v_t \sim \ell\dot{\gamma}$ one expects a time-independent stress $\sigma \sim c_t\dot{\gamma}$ at small strains. Rather we obtain $\sigma \sim c_t\dot{\gamma}(t/c_t)^\epsilon$ with a small exponent $\epsilon \approx 0.1$ that embodies the time dependence of the stress. For the

contact velocities this would imply $v \sim (t/c_t)^{\epsilon/2}\ell\dot{\gamma}$; alternatively, for the contact displacements $\delta_t^2 \sim t^{2+\epsilon}$. The origin of such a behavior is currently unclear.

[1] C. Heussinger, Phys. Rev. E **102**, 022903 (2020).

[2] S. Torquato and F. H. Stillinger, Rev. Mod. Phys. **82**, 2633 (2010).

[3] J. Zhao, S. Li, R. Zou, and A. Yu, Soft Matter **8**, 1003 (2012).

[4] S. R. Williams and A. P. Philipse, Phys. Rev. E **67**, 051301 (2003).

[5] A. P. Philipse, Langmuir **12**, 1127 (1996).

[6] L. Onsager, Ann. N. Y. Acad. Sci. **51**, 627 (1949).

[7] D. Rodney, M. Fivel, and R. Dendievel, Phys. Rev. Lett. **95**, 108004 (2005).

[8] J. Blouwolff and S. Fraden, Europhys. Lett. **76**, 1095 (2006).

[9] C. R. Calladine, Int. J. Solids Struct. **14**, 161 (1978).

[10] A. Wouterse, S. Luding, and A. P. Philipse, Gran. Matter **11**, 169 (2009).

[11] L. Meng, Y. Jiao, and S. Li, Powder Technol. **292**, 176 (2016).

[12] L. Pournin, M. Weber, M. Tsukahara, J.-A. Ferrez, M. Ramaioli, and T. M. Liebling, Gran. Matter **7**, 119 (2005).

[13] R. S. Hoy, Phys. Rev. Lett. **118**, 068002 (2017); J. D. Dietz and R. S. Hoy, Soft Matter **16**, 6206 (2020).

[14] P. Langston, A. R. Kennedy, and H. Constantin, Comput. Mater. Sci. **96**, 108 (2015).

[15] C. Barbier, R. Dendievel, and D. Rodney, Phys. Rev. E **80**, 016115 (2009).

[16] J. G. Parkhouse and A. Kelly, Proc. R. Soc. London A **451**, 737 (1995).

[17] A. Ekman, A. Miettinen, T. Tallinen, and J. Timonen, Phys. Rev. Lett. **113**, 268001 (2014).

[18] J. E. Butler and B. Snook, Annu. Rev. Fluid Mech. **50**, 299 (2018).

[19] T. Nath and C. Heussinger, Eur. Phys. J. E **42**, 157 (2019).

[20] D. B. Nagy, P. Claudin, T. Börzsönyi, and E. Somfai, Phys. Rev. E **96**, 062903 (2017).

[21] V. V. Mahajan, J. Mehmood, Y. M. F. El Hasadi, and J. T. Padding, Chem. Eng. Sci.: X **3**, 100030 (2019).

[22] T. A. Marschall and S. Teitel, Phys. Rev. E **101**, 032907 (2020).

[23] T. A. Marschall and S. Teitel, Phys. Rev. E **100**, 032906 (2019).

[24] E. Azéma and F. Radjaï, Phys. Rev. E **81**, 051304 (2010).

[25] F. Tapia, S. Shaikh, J. E. Butler, O. Pouliquen, and E. Guazzelli, J. Fluid Mech. **827**, R5 (2017).

[26] R. E. Egres and N. J. Wagner, J. Rheol. **49**, 719 (2005).

[27] E. Brown, H. Zhang, N. A. Forman, B. W. Maynor, D. E. Betts, J. M. DeSimone, and H. M. Jaeger, Phys. Rev. E **84**, 031408 (2011).

[28] R. C. Hidalgo, B. Szabó, K. Gillemot, T. Börzsönyi, and T. Weinhart, Phys. Rev. Fluids **3**, 074301 (2018).

[29] P. A. Cundall and O. D. L. Strack, Géotechnique **29**, 47 (1979).

[30] E. Bitzek, P. Koskinen, F. Gähler, M. Moseler, and P. Gumbsch, Phys. Rev. Lett. **97**, 170201 (2006).

[31] A. W. Lees and S. F. Edwards, J. Phys. C: Solid State Phys. **5**, 1921 (1972).

[32] C. F. Schreck, N. Xu, and C. S. O'Hern, Soft Matter **6**, 2960 (2010).

[33] A. Bausch and K. Kroy, Nat. Phys. **2**, 231 (2006).

[34] B. Alberts, D. Bray, J. Lewis, M. Raff, K. Roberts, and J. D. Watson, *Molecular Biology of the Cell* (Garland Publishing, New York, 1994).

[35] R. C. Picu, Soft Matter **7**, 6768 (2011).

[36] J. Plagge, A. Fischer, and C. Heussinger, Phys. Rev. E **93**, 062502 (2016).

[37] C. Heussinger, B. Schaefer, and E. Frey, Phys. Rev. E **76**, 031906 (2007).